Research Square

Preprints are preliminary reports that have not undergone peer review.
They should not be considered conclusive, used to inform clinical practice,
or referenced by the media as validated information.

Inhibition of Notch1 Signal Promotes Brain Recovery by Modulating Glial Activity

Xiao zhu Hao
Huashan Hospital Fudan University Department of Radiology
Lu yi Lin
Huashan Hospital Fudan University Department of Radiology
Cheng feng Sun
Huashan Hospital Fudan University Department of Radiology
Chan chan Li
Huashan Hospital Fudan University Department of Radiology
Jing Wang
Huashan Hospital Fudan University Department of Radiology
Min Jiang
Huashan Hospital Fudan University Department of Radiology
Zhen wei Yao
Huashan Hospital Fudan University Department of Radiology
Yan Mei Yang (yym9876@sohu.com)
Department of Radiology of Huashan Hospital

Research

Keywords: Notch1, astrocyte, microglia, MCAO, DAPT, striatum, cortex, magnetic resonance imaging

Posted Date: June 29th, 2021

DOI: https://doi.org/10.21203/rs.3.rs-651228/v1

License: This work is licensed under a Creative Commons Attribution 4.0 International License.
Read Full License

Abstract

Background

Notch1 signaling inhibiton with N-[N-(3,5-difluorophenacetyl)-1-alanyl]-S-phenylglycine t-butylester] (DAPT) treatment could promote brain recovery and the intervention effect is different between striatum (STR) and cortex (CTX), which might be accounted for changed glial activities but the in-depth mechanism is still unknown. The purpose of this study was to identify whether DAPT could modulate microglial subtype shifts and astroglial-endfeet aquaporin-4 (AQP4) mediated waste solute drainage.

Methods

Sprague-Dawley rats (n=10) were subjected to 90min of middle cerebral artery occlusion (MCAO) and were treated with DAPT (n=5) or act as control with no treatment (n=5). Two groups of rats underwent MRI scans at 24h and 4 week following stroke, and sacrificed at 4 week after stroke for immunofluorescence (IF).

Results

Compared with control rats, MRI data showed brain recovery in ipsilateral STR but not CTX. And IF showed decreased pro-inflammatory M1 microglia and increased anti-inflammatory M2 microglia in striatal lesion core and peri-lesions of STR, CTX. Meanwhile, IF showed decreased AQP4 polarity in ischemic brain tissue, however, AQP4 polarity in striatal peri-lesions of DAPT treated rats was higher than that in control rats but shows no difference in cortical peri-lesions between control and treated rats.

Conclusions

The present study indicated that DAPT could promote protective microglia subtype shift and striatal astrocyte mediated waste solute drainage.

Introduction

Ischemic stroke is a leading cause of disability worldwide, and unfortunately bring functional and cognitive deficits to suffers in that there is no approved treatment for stroke recovery. Neuroinflammation, as a persistent response that starts with an initial inflammatory stimulu and becomes self-propagating when develops, had been put in the spotlight and might provide potentially endogenous reparative targets. As brain resident inflammatory cells, microglia and astrocytes were activated within hours and recruited to the lesion site following ischemia, forming a frontline of glial scar and playing biphasic roles depending on the dynamical and differential polarization, suggests a complex relationship between acute and chronic phases of stroke [1]. And when detrimental responses do not resolve properly, it may result in secondary neurodegeneration and dementia in stroke survivors [1]. Studies showded that Notch1 signaling play pivotal roles in inflammation process after stroke and may provide important targets for treatment of stroke [2-7].

Notch1 signaling, expressed in resident inflammatory cells, is initiated when ligands bind to Notch1 receptor, resulting in release and translocation of NICD into nucleus, where it directs the outcome of innate and adaptive immune responses [8-11]. In our previous study, we have detected that attenuation of Notch1 signaling could promote brain tissue recovery of striatum (STR) and reconstruction of corticospinal tract (CST) with DAPT treatment but not cortex (CTX) [12, 13], and what accounts for this discrepancy and the underlying pathological changes are still unknown. CTX, as gray matter, is mainly composed of neuron and astrocytes. While STR, where the inside part abundantly composed of white matter, mainly constitutes axonal tracts and interspersed with neurons and astrocytes. Following stroke, the damaged tissue undergoes liquefactive necrosis, which is toxic to viable tissue and is removed depending on the combination of astroglial paravascular clearance and microglial endocytosis in the adjacent tissue [14]. So whether the changed functions of astrocytes and microglia, by DAPT treatment, contributed to the recovery of brain tissue as well as the discrepancy between STR and CST deserves to be studied.

Resting and activated microglia distributed in ischemic core and boundary, and present as M1 or M2 subtype according to stimuli and environment [15, 16], that M1 microglia release pro-inflammatory chemokine such as IL1, IL6, TNFα while M2 microglia secret anti-inflammatory factors such as IL10, TGFβ The former subtype, by release of pro-inflammatory chemokine and up-regulation of aquaporin-4 (AQP4) expression in astrocytes, cause BBB disruption [17]. It even result in increase of A1 astrocytes [18, 19], which lose routine functions of astrocyte and release cytotoxic factors that reduce or alter the brain's reparative response [20-23]. Thus, the moderate phenotype transition from M1 to M2 would be valuable to ameliorate brain damage and promote brain recovery.

Astrocytes modulate the environment around neurons by releasing neurotransmitters and other extracellular signaling molecules, even trans-differentiating into functional neurons [24-27]. More importantly, in recent years, the glymphatic system (Glm), paralleling to the blood vasculature and representing the second circulation, become another spotlight of astrocytes [28]. Glm accounts for the clearance of interstitial fluid and other solutes not absorbed across postcapillary venules [28]. As the indispensable part of Glm, aquaporin-4 (AQP4) water channel polarized in the astrocytic endfeet to provide low-resistent pathway for fluid movement and facilitatethe influx of subarachnoid CSF from para-arterial spaces into the brain interstitium, as well as the subsequent clearance of ISF via convective bulk flow [28, 29]. Molecules present in necrosis can leak across the glial scar and are removed by paravascular clearance via astrocyte in the ischemic boundary [14]. Waste solutes would accumulate in brain because of mis-location of AQP4 off the astrocytes' endfeet [30]. There was study demonstrated that inhibition of Notch1 signal with DAPT could reduce deposits of cerebral toxins and improve sensory function after cerebral cortical infarction with reduced astrocytic activation [31]. Thus, changes of astrogliosis together with the corresponding AQP4 expression with DAPT treatment after stroke need to be further studied.

Comprehensive molecular and cellular changes resulted in macroscopically changes in magnetic resonance imaging (MRI), a popular and indispensable method, provide in vivo evaluation of damaged

brain tissue dynamically. Especially diffusion tensor imaging (DKI), sensitive to cellular changes in and around the lesion. Thus, the current work evaluated the MR changes of CTX and STR in vivo, and detected their corresponding glial changes in vitro, to elucidate the pathological changes and the underlying mechanism following DAPT treatment.

Materials And Methods

Animals

Adult Male Sprague-Dawley rats (260-270g) were obtained from Shanghai Experimental Animal Center of Fudan University. All procedures performed in this study were approved by Fudan University of Institutional Animal Care and Use Committee, and every effort was made to minimize suffering and to reduce the number of animalsused.

Experimental groups

To evaluate the proliferative response following treatment with the γ-secretase inhibitorat the subacute stage, rats were subjected to MCAO, treated by i.c.v administration (day4) of DAPT. Five rats of each subgroup were performed with MRI and the subsequent decapitation for immunofluorescence at 4w respectively. Figure1A shows the time schedule for experimental procedures in all groups (Fig. 1A).

Stroke model

Rats were anesthetized with an intraperitoneal injection of 10% chloral hydrate under spontaneous inspiration, and the body temperature was continuously monitored at 37°C ± 0.5°C during the surgical procedures. For all rats, the left middle cerebral artery (MCA) was occluded for 90 minutes. In details, rats were immobilized by a tooth holder and with binding of all limbs, followed by the insertion of a 4.0 silicon-coated polypropylene suture into the left internal carotid artery (ICA) through the external carotid artery (ECA) and common carotid artery (CCA) to block blood flow to the MCA. After 90 minutes, the filament was withdrawn from the ICA to allow reperfusion. The follow-up T2 MRI was acquired under the anesthetized circumstances to check the occlusion of the left hemisphere 24 hours post-stroke. The above procedure was identical to that in our previous study [32].

Administration of γ-secretase inhibitor

DAPT powder (Sigma-Aldrich, St. Louis, MO, USA), was dissolved in DMSO to prepare concentrations of 8.3 mg/ml. DAPT solution (0.03 mg/kg) was stereotactically injected into the lateral cerebral ventricle (LV) for treated group rats at day 4 after stroke. Rats were anesthetized and placed in a stereotactic holder and immobilized by earplugs and a toothholder. A burr hole was drilled in the skull, 4.0 mm deep into the pial surface, -2.0 mm anteroposterior relative to the bregma, and 1.0 mm lateral to the midline, according to Paxinos and Watson atlas (1998) [33]. With a 2.0 μl Hamilton syringe, DAPT administration was finished within 3 minutes and the needle was left in place for 4 minutes to prevent leakage along the injection track.

Magnetic resonance imaging

Multimodal MRI of rats, including relaxation time imaging and diffusion imaging, was conducted in each group rats. Prior to MRI, animals were anesthetized by the same procedure as described for the MCAO model (see above). The body temperature was continuously monitored at 37°C ± 0.5°C, at the same time, blood oxygen saturation and heart rate were monitored during MRI procedures. The MRI measurements were performed in a 3.0-T horizontal magnet (Discovery MR750, GE Medical Systems, Milwaukee, WI) with a 60-mm-diameter gradient coil (Magtron Inc., Jiangyin, China).

T2-weighted MR images were acquired by a fast spin-echo sequence with the following parameters: Repetition Time (TR)/Echo Time (TE) = 4,000 ms/96 ms, scan time = 3 min, Field of View (FOV) = 6 cm × 6 cm, matrix = 256 × 256, slice thickness (ST) = 1.8 mm, spatial resolution = 0.24 × 0.24 × 1.8 mm^3, inter-slice distance = 2 mm, number of slices = 15, and number of average (NA) = 2.

For DKI acquisition, diffusion weighted images were acquired with TR/TE = 4,000 ms/84 ms, FOV = 6 cm × 6 cm, ST = 1.8 mm, inter-slice distance = 2 mm, matrix = 64 × 64, in-plane voxel size = 234 μm × 234 μm, NA = 4. The number of gradient directions was 15 with the duration of each of the diffusion gradients (δ) being 4 ms with a temporal spacing of 23 ms (Δ) between the two diffusion gradients. Two b-values (1,000 s/mm^2 and 2,000 s/mm^2) were acquired for each direction following the acquisition of five images acquired at b = 0 s/mm^2.

Fluorescence immunolabeling and confocal microscopy

Removed brain samples of rats were post-fixed in 4% paraformaldehyde for 24 hours, and then were vitrified in 20% and 30% sucrose solutions for 24 hours and 3 days, respectively. Coronal brain sections of all rats were obtained using a cryostat (RM2135, Leica). Immunofluorescence was performed on cryosections (30 μm): approximately 1.70 to -4.80 mm to Bregma according to Paxinos and Watson atlas [33]. In details, sections were washed three times with phosphate buffered saline (PBS, pH = 7.4). Sections were then blocked from non-specific binding with 10% normal donkey serum in PBS containing 0.3% Trition-X-100 (Sigma-Aldrich, St. Louis, MO, USA) for 2 hours at room temperature. Primary antibodies used were: (1) mouse anti-GFAP (1:300, GeneTex, Texas, USA); (2) mouse anti-CD11b (1:200, AbDSerotec, Kidlington, UK); (3) mouse anti-Iba1 (1:500; Abcam, Cambridge, MA, United States); (4) goat anti-CD206 (1:100, R&D systems, Minneapolis, MN, USA); (5) mouse anti-inos (1:100, Abcam, Cambridge, MA, United States); (6) mouse anti-MBP (1:500, Abcam, Cambridge, MA, United States); (7) NeuN (Biosensis, Thebarton, SA, Australia; 1:250); (8) mouse anti-AQP4 (1:200, Abcam, Cambridge, MA, United States). Primary antibodies were incubated overnight with sections at 4°C. Balanced at room temperature for about 30 minutes, sections were rinsed with PBS for 5 minutes with 3 times. Sections were then incubated with secondary antibodies as Alexa Fluor 488- and 568- conjugated donkey anti-mouse, anti-rabbit, or anti-goat (Life Technologies, Carlsbad, CA, USA; 1:200). Rinsed with PBS for 5 minutes with 3 times, sections were then counterstained with DAPI (Sigma-Aldrich, St. Louis, MO, USA; 1:1000). At last, all the sections were rinsed with PBS for 5 minutes with 3 times, and cover slipped with mounting

medium. Sections from different groups were respectively processed together in the same batches to minimize staining variability.

Image processing and quantitative analysis

MRI

Regions of interest (ROIs) including STR and CTX were selected for analysis of T2 signal intensity (SI) or DKI parameters. For T2 SI analysis, ROIs were placed on the whole lesion of STR and CTX with the T2 MR image. To assess the DKI parameters, axial T2 MR images were used for anatomical references to assess the topography of infarction. DKI measurement of MK, Ka and Kr were also analyzed in whole lesion of STR and CTX. Contralateral ROI regions were drawn on the contralateral hemisphere according to the size and shape of the ipsilateral ROIs. Entire ROI analysis was repeated twice to ensure reproducibility of the results. The percent change of every parameter value was computed as: $100 \times (X_i - X_c) / X_c$, where X represents an averaged metric. Figure1B shows ROIs for quantitative analysis in all rats (Fig. 1B)

Immunostaining

For histological images, sections were scanned with the ×20 primary objective of a Vslide scanning microscope (Nikon, Chiyoda,Tokyo, Japan) with filter sets for DAPI (EX350/50-EM470/40), FITC (EX493/16-EM527/30), and FRITC(550,620). Initial captures were stitched into Vslide software to create the integrated images of the whole brain. All the images were acquired with a resolution of 1024 × 1024 pixels using constant values for laser power, pinhole, digital gain, offset, and scan speed. With Image J (National Institutes of Health, Bethesda, MD, USA), the acquired images were semi-quantitatively measured by optical density of positively stained cells of the selected ROI. In control and DAPT treated rats, the intensity of all the immunofluorescent markers, including GFAP, CD11b, Iba1, CD206, inos, NeuN, MBP, in ischemic boundary or core of STR and CTX were calculated. Each value was also calculated in the contralateral site equivalent to the ipsilateral ROIs. The value of GFAP was computed as Xi/Xc , and other values were computed as: $100 \times (X_i - X_c) / X_c$, where X represents an averaged metric.

AQP4 expression polarity was analyzed as previous study described [34], that we set the threshold of each image at two different levels—a high and a low stringency threshold. The low-stringency threshold defined the overall area of AQP4 immunoreactivity, whereas the high-stringency threshold defined the area of intense AQP4 immunoreactivity, expressed in perivascular endfeet. The value, generated from the ratio of low-stringency area to high-stringency area, was used to define “AQP4 polarity”. The high value indicates greater perivascular AQP4 proportion, whereas the low value indicates more evenly distributed AQP4 expression. Each value was calculated in the contralateral site equivalent to the ipsilateral ROIs and was also computed as: $100 \times (X_i - X_c) / X_c$, where X represents an averaged metric.

Statistical Analysis

Unpaired t-tests were performed for two groups comparison. In statistical tests, differences were considered significant when $P < 0.05$ and data were presented as mean ± SD. Statistical analysis was performed using Prism, version 6.0 (GraphPad Software Incorporated, La Jolla, CA, USA).

Results

T2 SI changes in ischemic lesion

T2W images of two group rats showed that the ischemic lesion was formed and presented hyperintensity, which showed a good consistency between control group and treated group 24 hours following ischemia. Then 4 weeks after stroke, two group rats showed different changes in T2 SI (Fig.2A), that T2 SI percent changes in STR was significantly lower in treated group than that in control group ($P < 0.01$) (Fig.2A, B). However, for CTX at 4 weeks after stroke, the cystic region was formed in both control and treated rats, and there was no statistical difference of the percent change of T2 SI between two groups (Fig.2A, B).

DKI parameter changes in ischemic lesion

Based on the results detected by T2 MR images, we next measured the microstructural differences between rats with or without DAPT treatment, combining with statistical analysis of diffusion parameters (Fig.2A, C, D, E). MK, Ka and Kr showed more recovery of STR in treated rats, which showed statistical differences between two groups (MK, $P < 0.01$; Ka, $P < 0.01$; Kr, $P < 0.01$) (Fig. 2C, D, E). And for ipsilateral CTX, there was no statistical difference between rats with or without DAPT treatment 4 weeks after stroke (Fig. 2C, D, E).

Neuronal and axonal changes in ischemic boundary

We further analyzed the immunoreactivity of MBP and NeuN (a protein present in the myelin sheath surrounding axons and neurons respectively) in neural pathway of STR and CTX. In ipsilateral STR, axonal bundles were located in ischemic lesion and boundary, which is more sparsely in ischemic lesion of control rats but more integrated in that of DAPT treated rats, and the intensity of MBP in the whole striatal ischemic lesion are higher in treated rats than that in control rats ($P < 0.001$) (Fig.3A, A1, B, B1, E). And for ipsilateral CTX, the axonal bundles were mainly located in ischemic boundary but barely in lesion core, and there is no difference of the intensity of MBP between treated rats and control rats (Fig. 3C, C1, D, D1, E).

We next analyzed the staining intensity of NeuN in the whole ischemic lesion of two group rats. Our results showed that neurons significantly decreased in ipsilateral hemisphere and barely existed in CTX of both control and treated rats (Fig. 3C, C2, D, D2, F) but more survived in ipsilateral STR in DAPT treated rats than that in control rats ($P < 0.05$) (Fig.3A, A2, B, B2, F).

Astrocytic proliferation and AQP4 polarization in ischemic boundary

GFAP was used to study reactive astrogliosis within the perilesional area in both STR and CTX. Responding to ischemia, the astrocytic cell load significantly increased with hypertrophic body and longer extending processes (Fig.4A) in peri-lesions, and immunofluorescence images of GFAP showed that there was no difference of astrocytic cellular shape and density in CTX between DAPT treated and control group (Fig.4B1, B2–E) but this difference appeared in STR. Astrocytes in striatal peri-lesions of control rats showed compact cell density with hypertrophied cell body and intermingled processes, forming scar barrier around the lesion core (Fig.4C1). Following DAPT treatment, the glial scar is also exist but the shape of astrocytes showed more resemblance to that in context without ischemia stimuli (Fig.4C2), and statistical analysis showed lower density of striatal peri-lesions in DAPT treated rats (Fig.4E). To study whether the drainage function changes caused by astrocytes, we also analyzed the AQP4 polarity in peri-lesions, adjacenting to the glial scar. Results showed that there was no statistical difference of AQP4 polarity in cortical peri-lesions between two groups (Fig. 4B1, B2, F), however, in striatal peri-lesions, it was higher in DAPT treated rats (Fig. 4C1, C2, F).

Microglial activity and subtype shift in and around ischemic lesion

We have detected that microglia in treated rats was reversely more activated and being ramified with more processes in DAPT treated rats [12]. Then in this study, we futher analyzed the subtype shift of microglia in rats with and without DAPT treatment. Be consistent with the previous result, microglia was diffusively located in both peri-lesion and ischemic core and was more activated following DAPT treatment, while Iba1, one marker of both resting and activated microglia, showing no statistical differences between treated and control rats (Fig.5A, D, 6E, 7A, B, G). Both CD206 and inos, being markers of M2 and M1 microglia respectively, were expressed in ischemic core and peri-lesions of STR and CTX following ischemia. In STR, for CD206, the percent change of IF intensity in peri-lesions (Fig.5G, G1, H, H1) and ischemic core (Fig.5I, I1, J, J1) was significantly higher in treated rats than that in control rats (STR peri-, $P < 0.001$; STR core, $P < 0.001$) (Fig.6F). Meanwhile for inos, the percent change of IF intensity in peri-lesions (Fig. 6A, B) and ischemic core (Fig. 6C, D) was oppositely lower in treated rats than that in control rats (STR peri-, $P < 0.001$; STR core, $P < 0.001$) (Fig.6G). Unfortunately in the lesion of CTX, there was barely cellular activities, thus we only analyzed the inflammatory responses of peri-lesions (Fig. 7A, B). For CD206 (Fig. 7C, D) and inos (Fig. 7E, F), similar to that in STR, the percent change of IF intensity was higher and lower in treated rats than that in control rats respectively (CD206, $P < 0.001$; inos, $P < 0.001$) (Fig. 7H, I).

Discussion

DAPT treatment could ameliorate striatal brain edema and promote brain tissue recovery, that MR parameters showed relative recovery of STR in treated group while deterioration in control group and there was no recovery of CTX [12]. In this current work, MR images showed that the recovered tissue was mainly located at the ipsilateral STR, that percent changes of T2 SI, MK, Ka and Kr of STR were more close to the baseline when compared with control rats. There was no recovery on CTX in both control and treated group. Meanwhile, the IF result showed promoted recovery of myelin sheath and more survival of

neurons in STR but not CTX. The axonal bundle is more integrated and the intensity of MBP in the whole striatal ischemic lesion is statistically higher in treated rats than that in control rats. At the same time, neurons are more survived in ipsilateral STR and the intensity of NeuN is more higher in treated rats than that in control rats. However, there was no statistical difference of MBP and NeuN in CTX between treated rats and control rats. The AQP4 polarity showed significant recovery in area adjacent to glial scar in striatal peri-lesions, however, there was no statistical difference of AQP4 polarity in cortical peri-lesions. Concern about microglial subtypes of M2 and M1, the percent change of IF intensity of CD206 in treated rats was higher in striatal lesion core and ischemic boundary of both STR and CTX following DAPT treatment, while the inos showed opposite changes.

What might account for the discrepancy in MRI between STR and CTX is the microstructural difference that CTX is mainly composed of neurons and astrocytes, while the inside part of STR abundantly constitutes white matter of axonal bundle with interspersed neurons and astrocytes. Neuron is more sensitive to ischemia, resulting in immediate and unreversible cell death, and our previous study also demonstrated that there is barely viable neurons in the lesion core [32], even with DAPT treatment [13]. But there was more viable neurons in the ischemic boundary following DAPT treatment [13], which could form or integrate into existed neural circuits. Except for neurons' self-sensitivity to ischemia, inflammatory responses of astrocytes and microglia exert dual influence on neurons, synapses and axons by releasing pro- or anti-cytokines.

As resident immune cells within the CNS, microglia are the first activated cells in brain parenchyma following insult, migrate to the infarcted area and produce inflammatory cytokines to initiate an immune response, resulting in neural destruction as well as repair. And different types of microglia were triggered by ischemia and inflammation, termed 'M1' and 'M2', and the delicate balance between microglial subtype number is crucial to the fate of damaged brain tissue [16, 35-37]. Following ischemia, microglia diffusively located within the entire lesion, similar to astrocytes, assuming multiple neuroinflammatory roles within ischemic core and boundary [38]. Recent studies have shown that Notch-signaling contribute towards the activation of microglia, and treatment with DAPT could attenuate the expression of proinflammatory mediators of IL-1β and TNFα, which were markers of M1 microglia [4]. In this study we furthe analyze microglial activities and results indicated that pro-inflammatory M1 microglia was attenuated and anti-inflammatory M2 microglia was promoted.

Reactive astrocytes following cerebral ischemia were also regulated by Notch1 signaling. Notch1 signaling affects a unique subpopulation of proliferative reactive astrocytes that localize adjacent to the infarct and that regulate the peri-infarct area after stroke [2]. Astrocytes serve as prevention of immune cells invasion, phagocytosis of synapses, clearance of debris and dead cells in injured brain, repairation of the BBB, formation of a scar to enclose, elimination of the necrotic lesion injuries , and promotion of regrowth of the severed axons [39, 40]. Astrocytes respond diversely according to the extent of ischemia, showing gradually morphological and functional changes from close to distant peri-lesions. In our studies with 90 minutes occlusion of MCAO, there was no viable astrocytes in the ischemic core, which was only proliferated around the lesion with elongated and hypertrophied processes paralleling with or

projecting into the lesion core [32], which was consistent with other studies [41]. The mis-polarization of AQP4 from astrocytic endfeet impaired the glymphatic clearance [18], resulting in clearance failure of waste solutes of the ischemic lesion. In our study, we detected that attenuating Notch1 signal could modify astrocytic proliferation. The shape of astrocyte in DAPT treated rats was more consistent with ones in normal brain tissue, while presenting hypertrophied cell bodies and elongated processes in control rats. DAPT treatment might ameliorate the mis-location of AQP4 and maintain clearance function of glymphatic system.

A better understanding of the signaling mechanism that induce different types of microglia and reactive astrocytes will be an important step toward the development of drugs that allow us to control and harness glial cells to promote repair in disease. Notch1 signal, playing an crucial role in this process, would promote detrimental microglia to the protective subtype ones and maintain normal function of Glm dominated by astrocytes. However, whether subtypes of astrocytes also shifted from toxic A1 subtype to protective A2 subtype and thus contributed to the proper localization of AQP4 on the endfeet of astrocytes need to be further studied.

Conclusion

In this study, we detected that Notch1 signal inhibition with DAPT treatment could promote ischemic brain tissue recovery in STR but not CTX. Promotion of anti-inflammatory M2 phenotype and inhibition of pro-inflammatory M1 phenotype of microglia was one factor of damaged brain tissue recovery with DAPT treatment. And another contributor to striatal brain recovery was maintenance of AQP4 polarity in astrocytes, which not occurs in CTX and might accounts for the discrepancy of MRI as well as pathological changes between STR and CTX following DAPT treatment.

Abbreviations

SVZ: subventricular zone; aSVZ: anterior subventricular zone; NICD: Notch intercellular domain; AQP4: aquaporin-4; Glm: glymphatic system; DAPT: N-[N- (3,5-difluorophenacetyl)-1-alanyl]-S-phenylglycine t-butylester; MCAO: middle cerebral artery occlusion; MRI: magnetic resonance imaging; DKI: diffusion kurtosis imaging; IF: immunofluorescence; MCA: middle cerebral artery; CCA: common carotid artery; ECA: external cerebral artery; ICA: internal cerebral artery; LV: lateral ventricle; TR: Repetition Time; TE: Echo Time; FOV: Field of View. ST: slice thickness; NA: number of average; SI: signal intensity; PBS: phosphate buffered saline; ROI: region of interest; CNS: central nervous system; STR: striatum; CTX: cortex; MK: mean kurtosis; Ka: axonal kurtosis; Kr: radial kurtosis; SD: standard deviation; CST: corticospinal tract

Declarations

Ethics approval and consent to participate

The experiments were approved by Fudan University Institutional Animal Care and Use Committee (SCXY 2007–0002).

Consent for publication

Not applicable.

Availability of data and materials

All material used in this manuscript will be made available to researchers subjected to conficonfidentiality.

Competing interests

The authors declare no competing financial interests.

Fundings

This study was supported by the grant of National Natural Science Foundation of China (No. 81801660), the grant of National Natural Science Foundation of China (No. 81771788) and Shanghai Pujiang Program (20PJ1402200).

Authors' contributions

XZH carried out the animal experiments, performed the MR scanning and histological analysis, and drafted the manuscript. LLY and CFS carried out the animal experiments and performed the MR scanning. CCL and JW carried out the animal experiments and processed the MR imaging. ZWY supervised the MR imaging. MJ performed the histological analysis. YMY instructed the study protocol and revised the manuscript. All of the authors read and approved the final manuscript.

Acknowledgments

Not applicable.

References

1. Zera KA, Buckwalter MS: **The Local and Peripheral Immune Responses to Stroke: Implications for Therapeutic Development.** *Neurotherapeutics* 2020, **17:**414-435.

2. Shimada IS, Borders A, Aronshtam A, Spees JL: **Proliferating Reactive Astrocytes Are Regulated by Notch-1 in the Peri-Infarct Area After Stroke.** *Stroke* 2011, **42:**3231-3237.

3. **Notch Signaling in the Central Nervous System with Special Reference to its Expression in Microglia.** *CNS & Neurological Disorders - Drug Targets* 2013.

4. Wei Z, Chigurupati S, Arumugam TV, Jo DG, Li H, Chan SL: **Notch Activation Enhances the Microglia-Mediated Inflammatory Response Associated With Focal Cerebral Ischemia.** *Stroke* 2011, **42:**2589-2594.

5. Grandbarbe L, Michelucci A, Heurtaux T, Hemmer K, Morga E, Heuschling P: **Notch signaling modulates the activation of microglial cells.** *Glia* 2007, **55:**1519-1530.

6. Todd N. Eagar, Qizhi Tang, Michael Wolfe, Yiping He, Warren S. Pear, Jeffrey A. Bluestone1: **Notch 1 Signaling Regulates Peripheral T Cell Activation.** *Immunity* 2004, **20:**407–415.

7. Arumugam TV, Chan SL, Jo DG, Yilmaz G, Tang SC, Cheng A, Gleichmann M, Okun E, Dixit VD, Chigurupati S, et al: **Gamma secretase-mediated Notch signaling worsens brain damage and functional outcome in ischemic stroke.** *Nat Med* 2006, **12:**621-623.

8. Selkoe D, Kopan R: **Notch and Presenilin: regulated intramembrane proteolysis links development and degeneration.** *Annu Rev Neurosci* 2003, **26:**565-597.

9. Kopan R: **Notch: a membrane-bound transcription factor.** *J Cell Sci* 2002, **115:**1095-1097.

10. Eagar TN, Tang Q, Wolfe M, He Y, Pear WS, Bluestone JA: **Notch 1 signaling regulates peripheral T cell activation.** *Immunity* 2004, **20:**407-415.

11. Monsalve E, Pérez MA, Rubio A, Ruiz-Hidalgo MJ, Baladrón V, García-Ramírez JJ, Gómez JC, Laborda J, Díaz-Guerra MJ: **Notch-1 up-regulation and signaling following macrophage activation modulates gene expression patterns known to affect antigen-presenting capacity and cytotoxic activity.** *J Immunol* 2006, **176:**5362-5373.

12. Hao XZ, Tian JQ, Yin LK, Zhang XX, Li CC, Feng XY, Yao ZW, Jiang M, Yang YM: **MRI detects protective effects of DAPT treatment with modulation of microglia/macrophages at subacute and chronic stages following cerebral ischemia.** *Mol Med Rep* 2017, **16:**4493-4500.

13. Hao XZ, Yin LK, Tian JQ, Li CC, Feng XY, Yao ZW, Jiang M, Yang YM: **Inhibition of Notch1 Signaling at the Subacute Stage of Stroke Promotes Endogenous Neurogenesis and Motor Recovery After Stroke.** *Front Cell Neurosci* 2018, **12:**245.

14. Zbesko JC, Nguyen TV, Yang T, Frye JB, Hussain O, Hayes M, Chung A, Day WA, Stepanovic K, Krumberger M, et al: **Glial scars are permeable to the neurotoxic environment of chronic stroke infarcts.** *Neurobiol Dis* 2018, **112:**63-78.

15. Ma Y, Wang J, Wang Y, Yang GY: **The biphasic function of microglia in ischemic stroke.** *Prog Neurobiol* 2017, **157:**247-272.

16. Hu X, Leak RK, Shi Y, Suenaga J, Gao Y, Zheng P, Chen J: **Microglial and macrophage polarization—new prospects for brain repair.** *Nat Rev Neurol* 2015, **11:**56-64.

17. Qin C, Zhou LQ, Ma XT, Hu ZW, Yang S, Chen M, Bosco DB, Wu LJ, Tian DS: **Dual Functions of Microglia in Ischemic Stroke.** *Neurosci Bull* 2019, **35:**921-933.

18. Liddelow SA, Guttenplan KA, Clarke LE, Bennett FC, Bohlen CJ, Schirmer L, Bennett ML, Münch AE, Chung WS, Peterson TC, et al: **Neurotoxic reactive astrocytes are induced by activated microglia.** *Nature* 2017, **541:**481-487.

19. Yun SP, Kam TI, Panicker N, Kim S, Oh Y, Park JS, Kwon SH, Park YJ, Karuppagounder SS, Park H, et al: **Block of A1 astrocyte conversion by microglia is neuroprotective in models of Parkinson's disease.** *Nat Med* 2018, **24:**931-938.

20. Zhao Y, Rempe DA: **Targeting astrocytes for stroke therapy.** *Neurotherapeutics* 2010, **7:**439-451.

21. Brumm AJ, Carmichael ST: **Not just a rush of blood to the head.** *Nat Med* 2012, **18:**1609-1610.

22. Gleichman AJ, Carmichael ST: **Astrocytic therapies for neuronal repair in stroke.** *Neurosci Lett* 2014, **565:**47-52.

23. Liddelow SA, Barres BA: **Reactive Astrocytes: Production, Function, and Therapeutic Potential.** *Immunity* 2017, **46:**957-967.

24. Fields RD, Stevens-Graham B: **New insights into neuron-glia communication.** *Science* 2002, **298:**556-562.

25. Khakh BS, Sofroniew MV: **Diversity of astrocyte functions and phenotypes in neural circuits.** *Nat Neurosci* 2015, **18:**942-952.

26. Duan C-L, Liu C-W, Shen S-W, Yu Z, Mo J-L, Chen X-H, Sun F-Y: **Striatal astrocytes transdifferentiate into functional mature neurons following ischemic brain injury.** *Glia* 2015, **63:**1660-1670.

27. Magnusson JP, Goritz C, Tatarishvili J, Dias DO, Smith EM, Lindvall O, Kokaia Z, Frisen J: **A latent neurogenic program in astrocytes regulated by Notch signaling in the mouse.** *Science* 2014, **346:**237-241.

28. Iliff JJ, Wang M, Liao Y, Plogg BA, Peng W, Gundersen GA, Benveniste H, Vates GE, Deane R, Goldman SA, et al: **A paravascular pathway facilitates CSF flow through the brain parenchyma and the clearance of interstitial solutes, including amyloid β.** *Sci Transl Med* 2012, **4:**147ra111.

29. Bechmann I, Galea I, Perry VH: **What is the blood–brain barrier (not)?** *Trends in Immunology* 2007, **28:**5-11.

30. Bronzuoli MR, Facchinetti R, Valenza M, Cassano T, Steardo L, Scuderi C: **Astrocyte Function Is Affected by Aging and Not Alzheimer's Disease: A Preliminary Investigation in Hippocampi of 3xTg-AD Mice.** *Front Pharmacol* 2019, **10:**644.

31. Zhang Y, Xing S, Zhang J, Li J, Li C, Pei Z, Zeng J: **Reduction of β-amyloid deposits by γ-secretase inhibitor is associated with the attenuation of secondary damage in the ipsilateral thalamus and sensory functional improvement after focal cortical infarction in hypertensive rats.** *J Cereb Blood Flow Metab* 2011, **31:**572-579.

32. Hao XZ, Yin LK, Zhang XX, Tian JQ, Li CC, Feng XY, Jiang M, Yang YM: **Combining systemic and stereotactic MEMRI to detect the correlation between gliosis and neuronal connective pathway at the chronic stage after stroke.** *J Neuroinflammation* 2016, **13:**156.

33. Paxinos G, Watson, C.: **The Rat Brain in Stereotaxic Coordinates.** *Academic Press, San Diego* 1998.

34. Sanchez-Bezanilla S, TeBay C, Nilsson M, Walker FR, Ong LK: **Visual discrimination impairment after experimental stroke is associated with disturbances in the polarization of the astrocytic aquaporin-4 and increased accumulation of neurotoxic proteins.** *Exp Neurol* 2019, **318:**232-243.

35. Li D, Lang W, Zhou C, Wu C, Zhang F, Liu Q, Yang S, Hao J: **Upregulation of Microglial ZEB1 Ameliorates Brain Damage after Acute Ischemic Stroke.** *Cell Rep* 2018, **22:**3574-3586.

36. Iadecola C, Anrather J: **The immunology of stroke: from mechanisms to translation.** *Nat Med* 2011, **17:**796-808.

37. Benakis C, Garcia-Bonilla L, Iadecola C, Anrather J: **The role of microglia and myeloid immune cells in acute cerebral ischemia.** *Front Cell Neurosci* 2014, **8:**461.

38. Eldahshan W, Fagan SC, Ergul A: **Inflammation within the neurovascular unit: Focus on microglia for stroke injury and recovery.** *Pharmacol Res* 2019, **147:**104349.

39. Bush TG, Puvanachandra N, Horner CH, Polito A, Ostenfeld T, Svendsen CN, Mucke L, Johnson MH, Sofroniew MV: **Leukocyte infiltration, neuronal degeneration, and neurite outgrowth after ablation of scar-forming, reactive astrocytes in adult transgenic mice.** *Neuron* 1999, **23:**297-308.

40. Anderson MA, Burda JE, Ren Y, Ao Y, O'Shea TM, Kawaguchi R, Coppola G, Khakh BS, Deming TJ, Sofroniew MV: **Astrocyte scar formation aids central nervous system axon regeneration.** *Nature* 2016, **532:**195-200.

41. Wanner IB, Anderson MA, Song B, Levine J, Fernandez A, Gray-Thompson Z, Ao Y, Sofroniew MV: **Glial scar borders are formed by newly proliferated, elongated astrocytes that interact to corral inflammatory and fibrotic cells via STAT3-dependent mechanisms after spinal cord injury.** *J Neurosci* 2013, **33:**12870-12886.

Figures

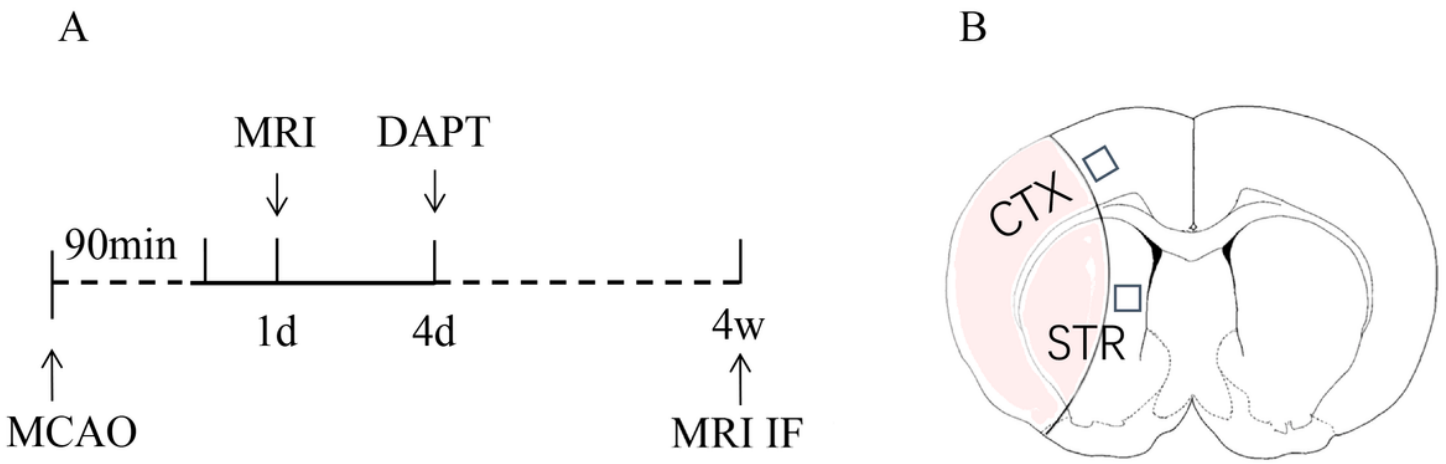

Figure 1

Experimental procedure. (A) Rats were subjected to MCAO, treated with or without DAPT, performed with MRI at 24h and 4w, and decapitated for immunohistochemical analysis at 4w after stroke. (B) Anatomical reference showing regions of interests (ROIs).

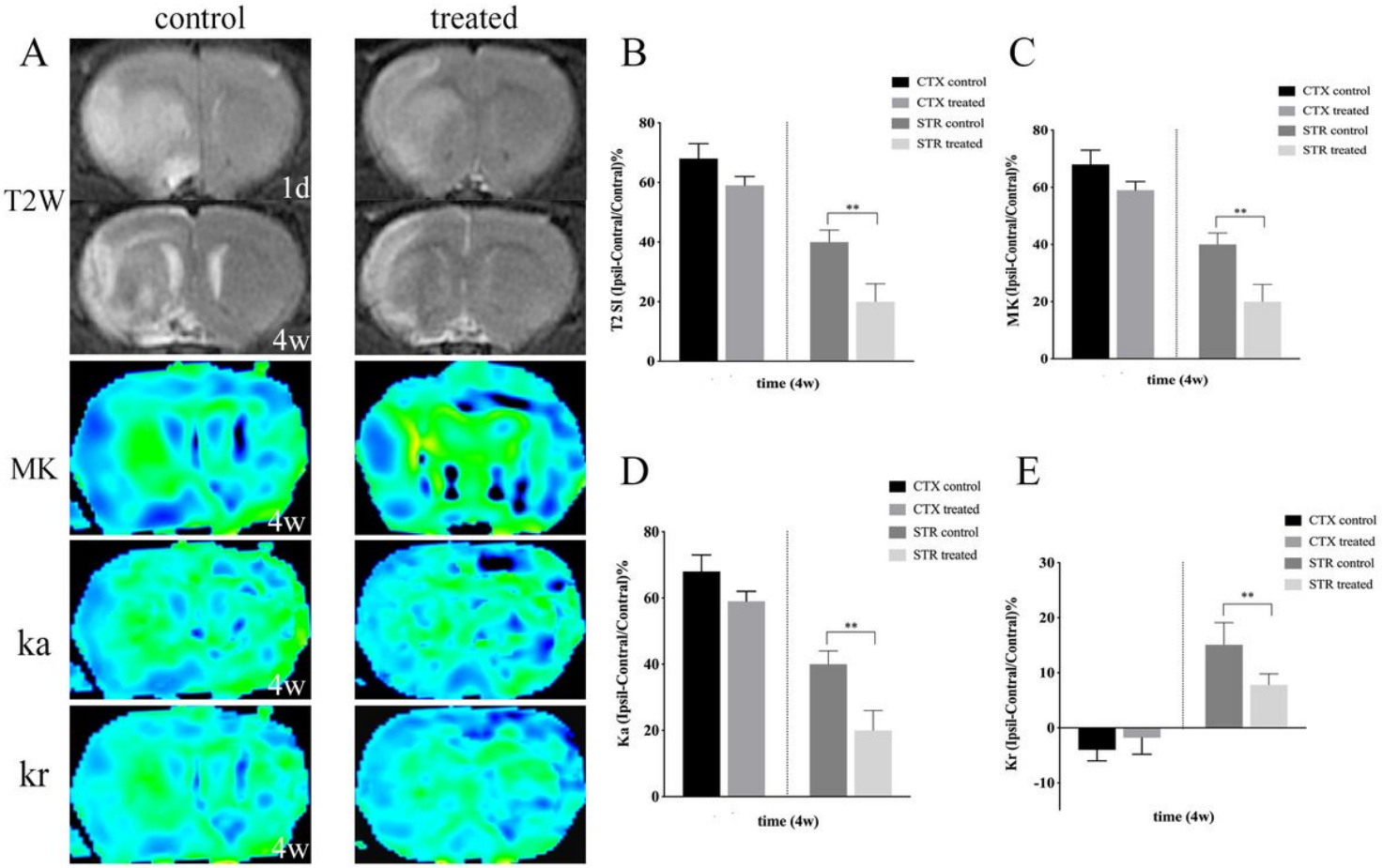

Figure 2

Effects of DAPT on structure changes of STR and CTX with T1W MRI and DKI maps after MCAO. (A) T1 MR images, MK, Ka and Kr maps in control and DAPT treated rats. (B, C, D, E) Comparisons of T2 SI (B), MK (C), Ka (D), Kr (E) of ischemic striatum and cortex between two group rats. STR: **P < 0.01, T2 SI, MK, Ka, Kr.

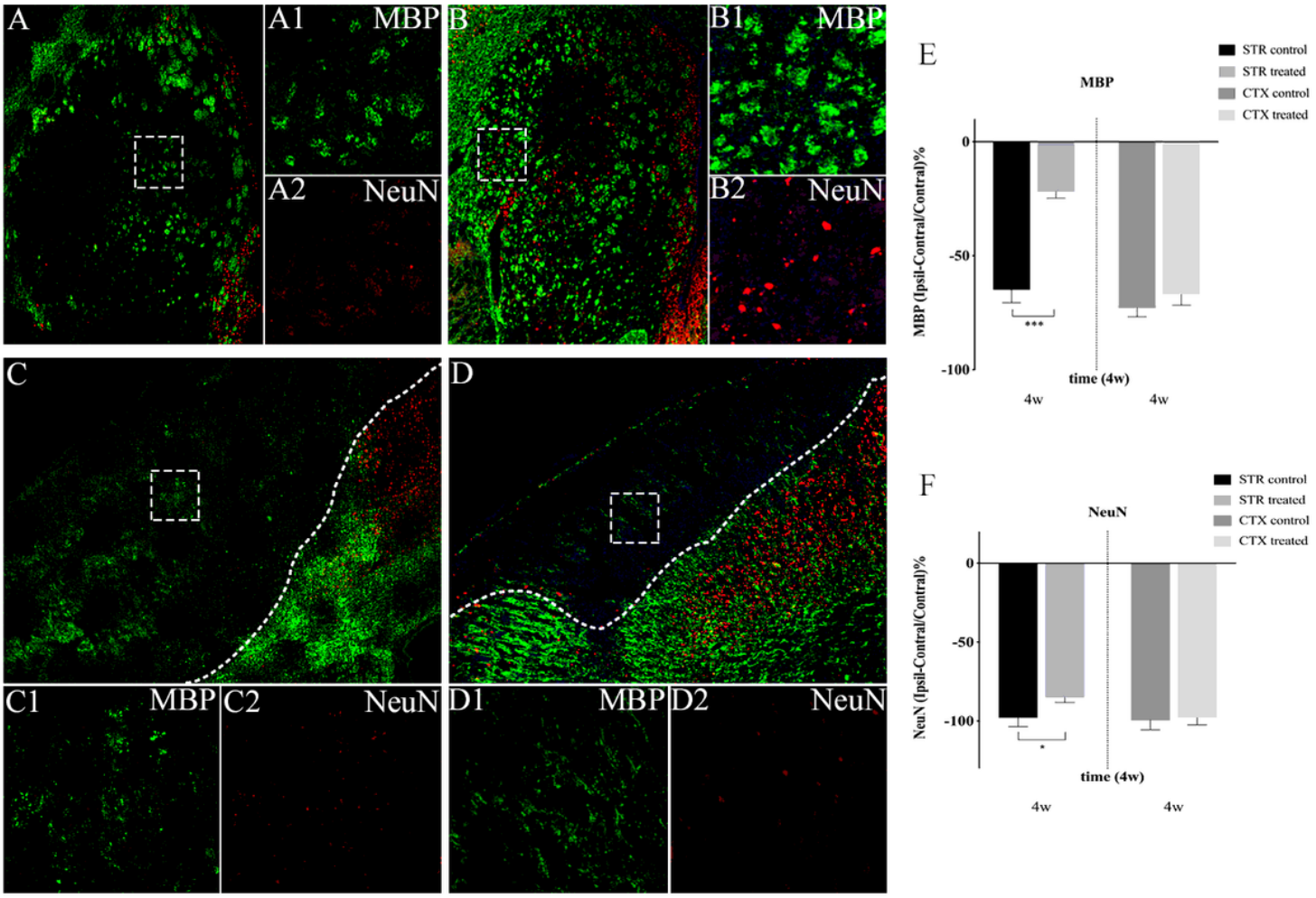

Figure 3

Effects of DAPT on MBP and mature neurons immunoreactivity of STR and CTX after MCAO. (A, A1, A2, B, B1, B2) Images show the location of MBP(+) and NeuN(+) cells in the ischemia area of STR in control (A, A1, A2) and DAPT treated rats (B, B1, B2). (C, C1, C2, D, D1, D2) Images show the location of MBP(+) and NeuN(+) cells in the ischemia area of CTX in control (C, C1, C2) and DAPT treated rats (D, D1, D2). (E, F) Comparisons of MBP (E) and NeuN (F) fluorescence intensity in STR and CTX between two group rats. STR: ***P < 0.001, MBP; *P < 0.05, NeuN.

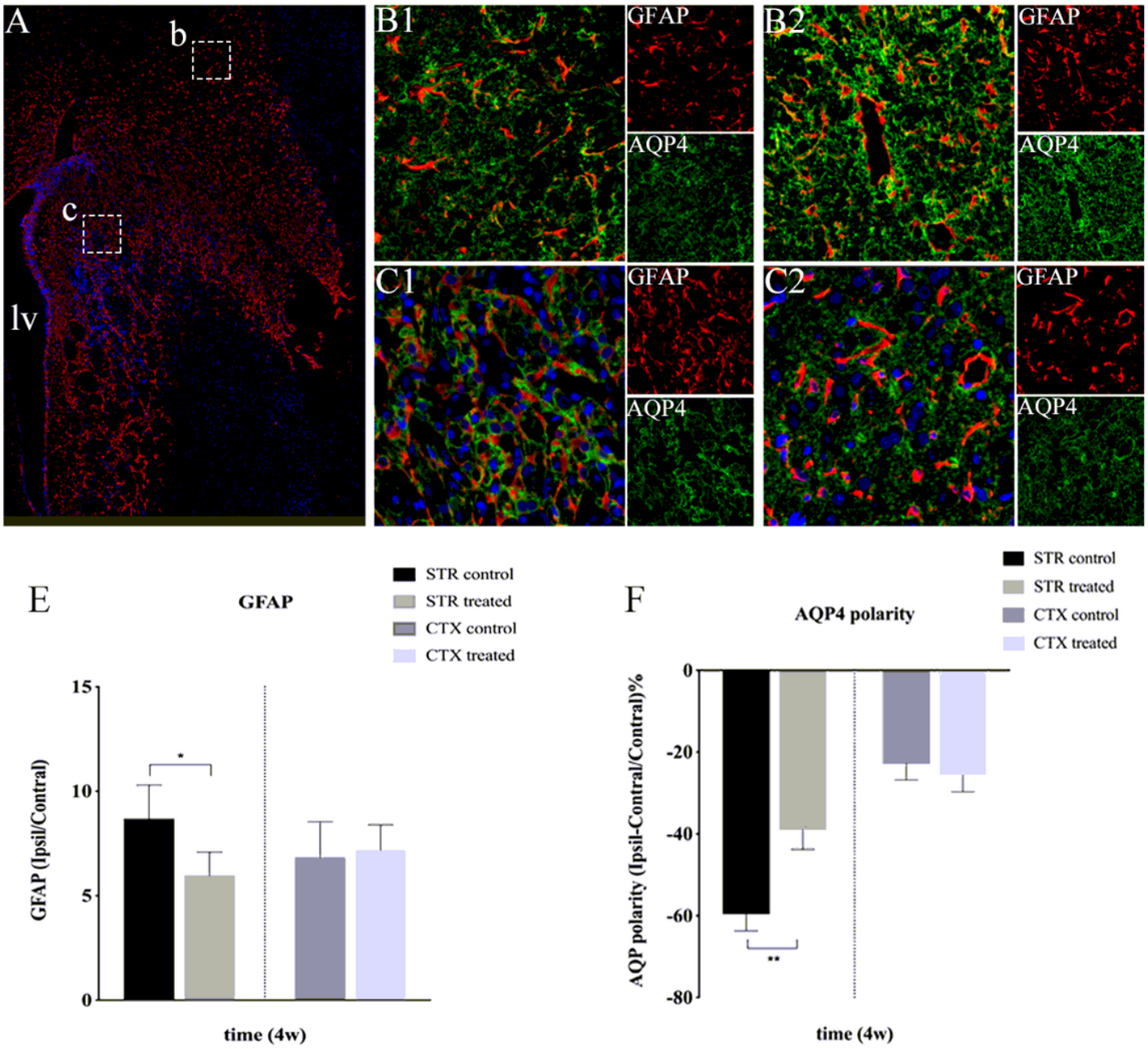

Figure 4

Effects of DAPT on astrocytes immunoreactivity and AQP4 polarity of STR and CTX after MCAO. (A) Image shows the location of GFAP (+) cells in peri-lesions of STR and CTX. (B1, B2) Enlarged images of GFAP/AQP4 of cortical peri-lesions in control (B1) and treated rats (B2), corresponding to the area within box b showed in image A. (C1, C2) Enlarged images of GFAP/AQP4 of striatal peri-lesions in control (C1) and treated rats (C2), corresponding to the area within box c showed in image A. (E, F) Comparisons of GFAP fluorescence intensity (E) and AQP4 polarity (F) in STR and CTX between two group rats. STR: *P < 0.01, GFAP; **P < 0.01, AQP4 polarity.

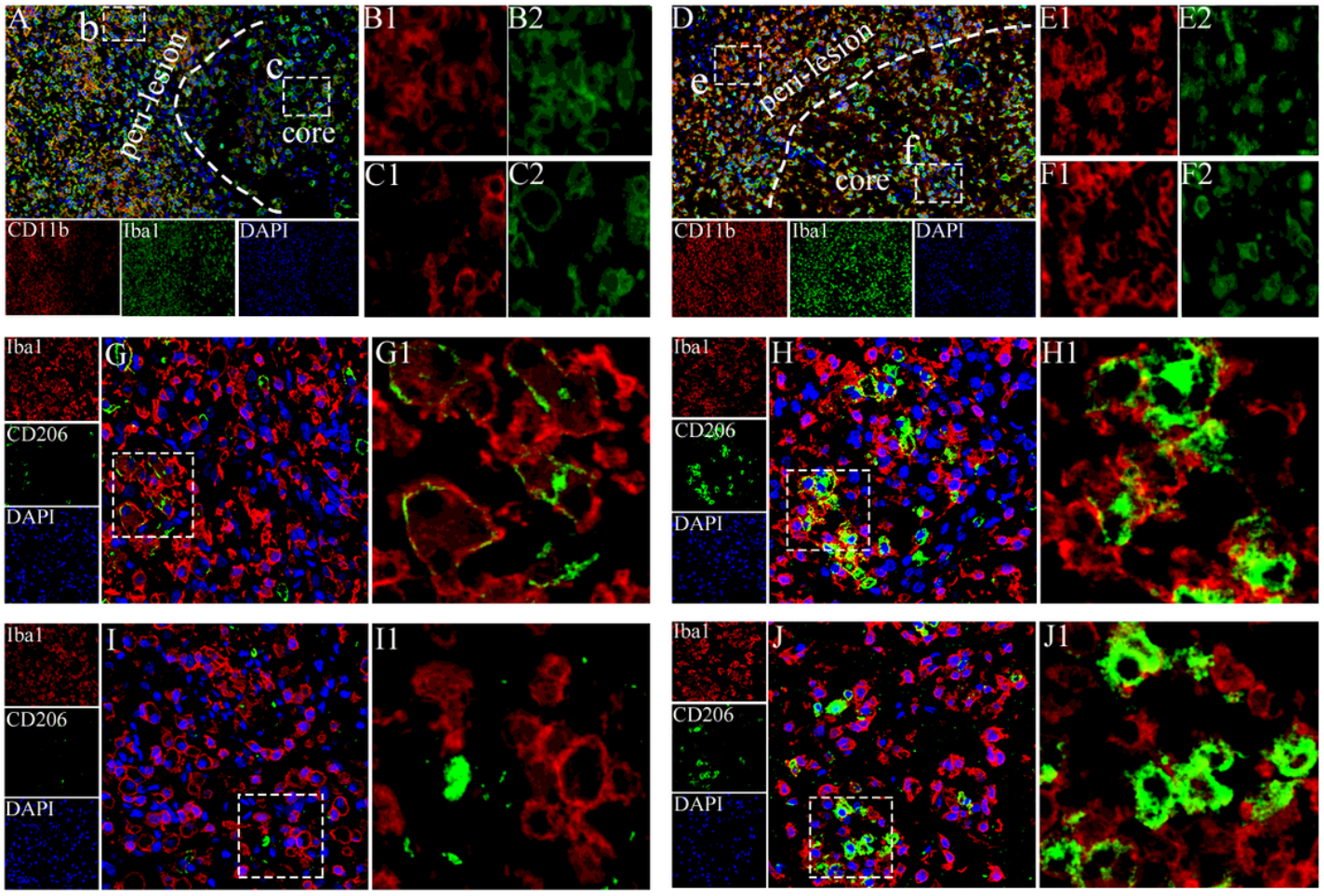

Figure 5

Effects of DAPT on microglia activity and subtype shift of STR after MCAO. (A, D) Images show the location of CD11b(+) and Iba1(+) cells in STR. (B1, B2, E1, E2) Enlarged images of CD11b and Iba1 in peri-lesions in control (B1, B2) and treated rats (E1, E2), corresponding to the area within box b and e respectively. (C1, C2, F1, F2) Enlarged images of CD11b and Iba1 in peri-lesions in control (C1, C2) and treated rats (F1, F2), corresponding to the area within box c and f respectively. (G, H, I, J) Images of Iba1/CD206(+) cells in peri-lesions (G, H) and ischemic core (I, J) in control and treated rats, together with enlarged images of Iba1/CD206 in peri-lesions (G1, H1) and ischemic core (I1, J1), corresponding to the area within boxes in G, H, I, J respectively.

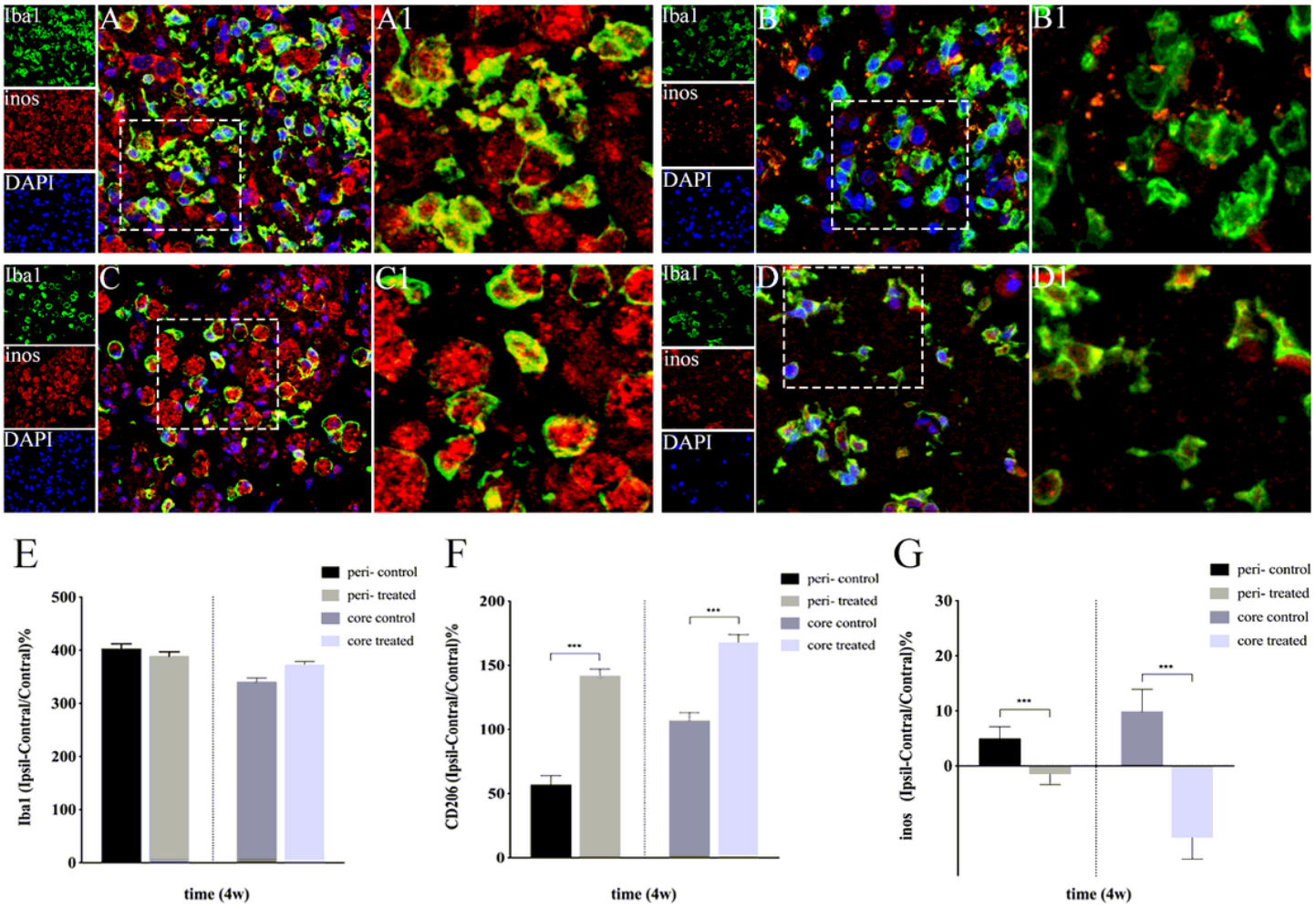

Figure 6

Effects of DAPT on microglia subtype shift of STR after MCAO. (A, B, C, D) Images show the location of iba1/inos(+) cells in peri-lesions (A, B) and ischemic core (C, D) of control and treated rats, together with enlarged images of Iba1/inos in peri-lesions (A1, B1) and ischemic core (C1, D1), corresponding to the area within boxes in A, B, C, D respectively. (E, F, G) Comparisons of Iba1 (E), CD206 (F), inos (G) fluorescence intensity in peri-lesions and ischemic core of STR and CTX between two group rats. CD206: ***P < 0.001, peri-lesion; ***P < 0.001, core; inos: ***P < 0.001, peri-lesion; ***P < 0.001, core.

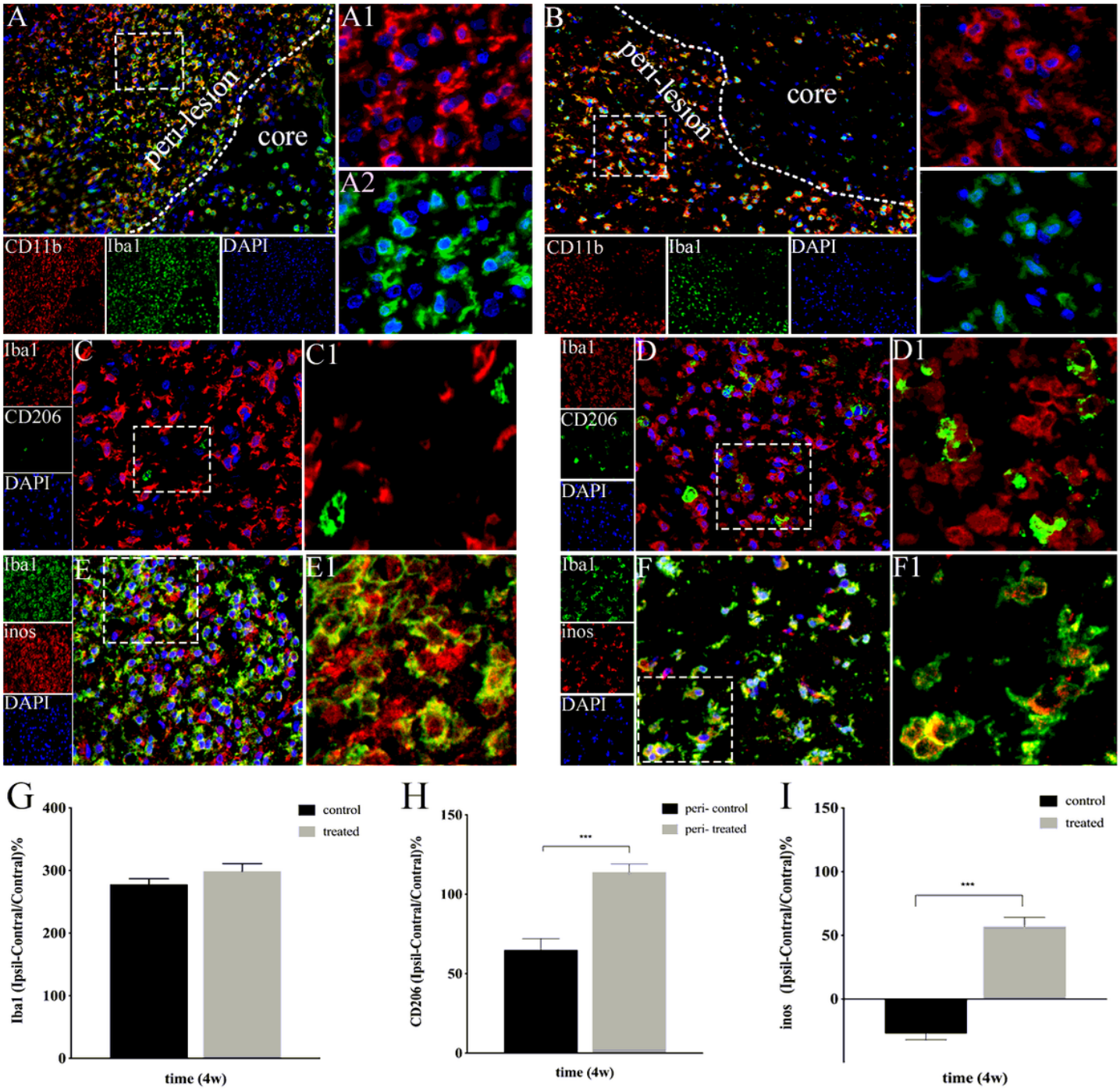

Figure 7

Effects of DAPT on microglia subtype shift in peri-lesions of CTX after MCAO. (A, B) Images show the location of CD11b(+) and Iba1(+) cells in peri-lesions of CTX in control (A) and treated (B) rats, together with enlarged images of CD11b (A1, B1) and Iba1 (A2, B2), corresponding to area within boxes of image A and B. (C, D) Images of Iba1/CD206(+) cells in cortical peri-lesions of control (C) and treated (D) rats, together with enlarged images of Iba1/CD206 (C1, D1), corresponding to area within boxes of image C and D respectively. (E, F) Images of Iba1/inos(+) cells in cortical peri-lesions of control (E) and treated (F) rats, together with enlarged images of Iba1/inos (E1, F1), corresponding to area within boxes of image E

and F respectively. (G, H, I) Comparisons of Iba1 (G), CD206 (H), inos (I) fluorescence intensity in peri-lesions of CTX between two group rats. CD206: ***P < 0.001; inos: ***P < 0.001.